Acta Mech Sin (2010) 26:365–370
DOI 10.1007/s10409-010-0345-4

RESEARCH PAPER

Calculation of Hugoniot properties for shocked nitromethane based on the improved Tsien's EOS

Bo Zhao · Ji-Ping Cui · Jing Fan

Received: 25 August 2009 / Accepted: 28 December 2009 / Published online: 25 April 2010

Abstract We have calculated the Hugoniot properties of shocked nitromethane based on the improved Tsien's equation of state (EOS) that optimized by "exact" numerical molecular dynamic data at high temperatures and pressures. Comparison of the calculated results of the improved Tsien's EOS with the existed experimental data and the direct simulations show that the behavior of the improved Tsien's EOS is very good in many aspects. Because of its simple analytical form, the improved Tsien's EOS can be prospectively used to study the condensed explosive detonation coupling with chemical reaction.

Keywords Equation of state · High pressures and temperatures · Shocked nitromethane · Hugoniot properties

1 Introduction

Thermodynamically complete equations of state (EOS) are important for understanding condensed matter response at high temperatures and high pressures [1]. Knowledge of the pressure–volume–temperature (P–V–T) states of condensed materials is needed for modeling composition of planetary interiors, phase transitions, and chemical reactions. Due to the limited availability of P–V–T data under extreme conditions, EOS developments often utilize simplified assumptions regarding thermodynamic variables and coefficients, and lead to the predictions of EOS with limited accuracy.

Earlier EOS developments were not adequate to fully meet physical behaviors. For instance, Cowperthwaite and Shaw [2,3] assumed that the specific heat c_v is a function of temperature only and the coefficient of thermal pressure $(\partial P/\partial T)_v$ is a constant. These assumptions, though thermodynamically consistent, were made due to a lack of available data or insight regarding material behaviors at higher pressure or temperature. With the greater availability of data, these assumptions are no longer appropriate.

Lysne and Hardesty's EOS [4] development utilized a numerical analysis of experimental data. They measured Hugoniot data for a range of different initial temperatures, and obtained a complete thermodynamic description of 0.1 MPa isobar. Using these data, they were able to obtain numerical values of $E(S, V)$ for region of P–V space bounded by their Hugoniot measurements. Values of thermodynamic variables and coefficients were then calculated numerically from $E(S, V)$ values.

In the EOS developed by Winey et al. [1], three material parameters were modeled as functions of temperature and volume: specific heat at constant volume C_v, coefficient of thermal pressure $(\partial P/\partial T)_v$, and isothermal bulk modulus B_T. These three parameters are sufficient to determine the Helmholtz potential for the system and lead to a complete EOS. Analytic expressions for these parameters were developed from the Hugoniot curve for an initial temperature, the isothermal compression curve for the same temperature and the isobaric thermodynamic data at 0.1 MPa. In addition to these experimental data, appropriate thermodynamic relationships were employed to ensure thermodynamic consistency and to optimally use the available data.

Tsien [5] developed a complete analytical equation of state for Lennard–Jones fluid at high temperatures and pressures. From molecular kinetic theory, the form of Tsien's EOS is

$$\frac{PV}{kT} = 1 + f\left(\frac{T}{\theta_I}, \frac{V}{V^*}\right), \tag{1}$$

B. Zhao · J.-P. Cui (✉) · J. Fan
Key Laboratory of High Temperature Gas Dynamics,
Institute of Mechanics, Chinese Academy of Sciences,
Beijing 100190, China
e-mail: yuzhong@imech.ac.cn

where P is pressure, T is temperature, V is the volume per molecule, k is Boltzmann constant, θ_I is the characteristic temperature of interaction, and V^* is the characteristic volume. For the Lennard–Jones (L–J) potential

$$u = 4\varepsilon\left[\left(\frac{D}{r}\right)^{12} - \left(\frac{D}{r}\right)^{6}\right], \tag{2}$$

where V^* is defined as $V^* = D^3$, and θ_I is defined as $\theta_I = \varepsilon/k$. Furthermore, according to the effects of imperfection of molecular size at very high temperature or at very large volume

$$\lim_{V\to\infty} f\left(\frac{T}{\theta_I}, \frac{V}{V^*}\right) = 0, \tag{3}$$

$$\lim_{T\to\infty} f\left(\frac{T}{\theta_I}, \frac{V}{V^*}\right) = 0. \tag{4}$$

With the general concept, all the equations of state for condensed materials must satisfy the conditions embodied in Eqs. (3) and (4). By using the tabulated values of compressibility factors given by Wentorf and collaborators [6], the approximate form of Tsien's EOS is

$$\frac{PV}{kT} = 1 + \frac{1}{0.278\varsigma - 0.177}, \tag{5}$$

where ς is a single variable and sufficient with

$$\varsigma = \left(\frac{T}{\theta_I}\right)^{1/6}\left(\frac{V}{V^*}\right). \tag{6}$$

Zhao and his coworkers [7] have given the numerical table of EOS at high temperatures and pressures based on elaborated calculations of molecular dynamics and correlated it with the improved Tisen's EOS

$$\frac{PV}{kT} = 1 + \frac{1}{0.103\varsigma - 0.006}, \tag{7}$$

$$\varsigma = \left(\frac{T}{\theta_I}\right)^{3/5}\left(\frac{V}{V^*}\right)^{7/2}. \tag{8}$$

In this study, we chose nitromethane as the object to test the validity of the improved Tsien's EOS. Nitromethane as a prototypical energetic material has been extensively investigated both in experimental and theoretical studies [1–4,8–13]. Thus, many elaborated experimental measurements and theoretical results are available and used for reference.

2 The fundamental quantities in EOS and in shocked nitromethane

2.1 L–J potential of nitromethane

To predict the thermodynamic functions of condensed matter at high pressures and temperatures by using the improved Tsien's EOS, the L–J potential of material must be determined. The L–J potential of nitromethane may be calculated by the polarizability, which can be deduced by refractive index based on Causius–Mosotti–Debye equation

$$\frac{n^2-1}{n^2+2} \times \frac{M}{\rho} = \frac{4}{3}\pi N\alpha, \tag{9}$$

where n is refractive index, N is Avogadro number, and α is polarizability. The polarizability of nitromethane α is equal to $6.29 \times 10^{-12}\,\mathrm{cm}^3$ at ambient conditions for $n = 1.3818$. Therefore, the L–J potential of nitromethane is derived from the polarizability using Drude model [14]

$$\varepsilon = \frac{1}{3} I \frac{\alpha^2}{D^6}, \tag{10}$$

where ε, D are the parameters of L–J potential, and I is the dissociation energy of nitromethane. The molecular diameter D is determined by the bond of structure (bond lengths and bond angles of nitromethane) and the Van der Waal radius. Here, we have $D = 4.4 \times 10^{-10}$ m, then the $\varepsilon/k = 300$ K for $I = 14$ eV. The L–J potential for nitromethane is examined by the isothermal compression curve using MD method in the following section.

2.2 Isothermal compression

To test the validity of the L–J potential of nitromethane at high pressures, we performed the isothermal compression simulation at ambient temperature in the pressure range of 0.1 MPa to 28.8 GPa.

The ensemble is used in which 1,000 L–J particles form a cubic cell with periodic boundary for the isothermal compression simulation. The classical motion equation is resolved by Verlet algorithm with accuracy of $O(\Delta t^4)$ in location calculation and of $O(\Delta t^2)$ in velocity calculation. The step of time is taken as $\Delta t = 1.0 \times 10^{-15}$ s. The pressure in equilibrium system is calculated by stress method [15] in the simulation. The L–J potential is truncated at $4.0D$.

The isotherm compression data of liquid nitromethane obtained is shown in Fig. 1. For the comparison, we also show the experimental data [4] and previous simulation results [16–18] in Fig. 1. At low pressures, all the MD data agree with experimental data reasonably. However, there is a big difference between MD data of Sorescu et al. [17] and Liu et al. [18] with our calculations in the high pressure regime. It is mainly due to the different potentials used in the simulations. In Sorescu's simulation, the interaction between particles is the pair-wise Bukingham potential which might be too weak to describe the strong repulsion when molecular liquids/solids are at high pressures. Liu et al. used CHARMM program and the potential was developed by Alper et al. [19]. Both our and Jones's MD simulations agree nicely with the experimental data, and have the same trend at high pressures.

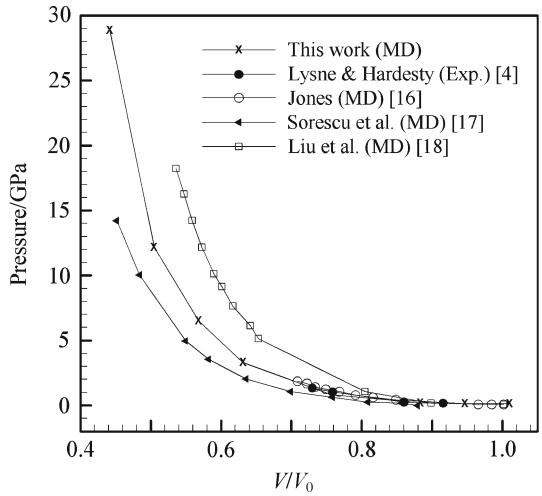

Fig. 1 Isothermal compression curve of liquid nitromethane at ambient temperature. Experimental data obtained by Lysne and Hardesty [4]. Other data from MD simulation (Refs. [16–18] and this work)

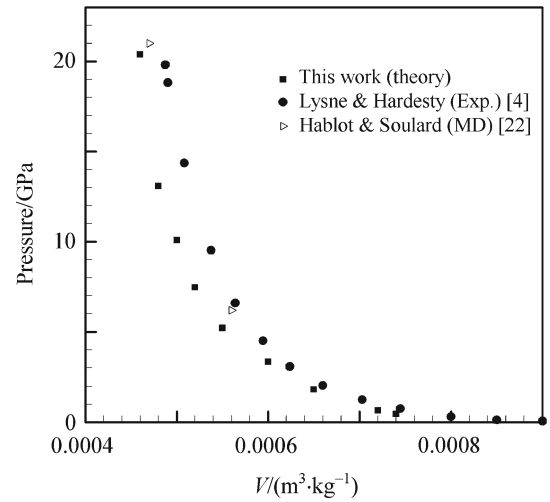

Fig. 2 Pressure along the Hugoniot curve

The discrepancy of pressures between our simulations and experiments is within 4.8% in experimental regime. We also obtained the isothermal compression data for $V/V_0 \leq 0.7$, which are not available in experiments and in Jones's work. The isothermal compression shows that the L–J potential chosen by us for nitromethane at high pressures is appropriate.

2.3 Determination of the thermodynamic functions

Let us consider a steady shock wave propagating to stationary material at the atmospheric pressure. The Hugoniot jump relations, which correlate the state ahead the shock of material (denoted by the subscript 0) with the state of post shock, are

$$\rho(U_s - U_p) = \rho_0 U_s, \tag{11}$$

$$P + \rho(U_s - U_p)^2 = P_0 + \rho_0 U_s^2, \tag{12}$$

$$h + \frac{1}{2}(U_s - U_p)^2 = h_0 + \frac{1}{2}U_s^2, \tag{13}$$

where ρ, U_s, U_p, P, and h are the density, the shock velocity, the particle velocity behind shock, the pressure, and the enthalpy, respectively. h_0 is obtained by direct MD simulation. By using the improved Tsien's EOS (Eqs.7, 8), the corresponding enthalpy is

$$h - h_\infty = \frac{41}{35}k\frac{1}{0.103\varsigma - 0.006}, \tag{14}$$

where h_∞ is the enthalpy of a perfect gas. The enthalpy and the specific heat at a constant pressure of perfect nitromethane gas have been calculated by Burcat [20]. From the data of enthalpy obtained by Burcat, we have the linear relationship between temperature and enthalpy for $T \geq 800$ K

$$h_\infty = h_{\infty 0} + C_P T, \tag{15}$$

where $h_{\infty 0}$ is the enthalpy of perfect gas at the temperature of initial state, and C_P is a constant of constant-pressure specific heat. The specific heat at a constant volume is also composed of the perfect part ($C_{v\infty}(T)$) and the imperfect one

$$C_v(v, T) - C_{v\infty}(T) = \frac{6}{35}k\frac{0.0412\varsigma - 0.006}{(0.103\varsigma - 0.006)^2}. \tag{16}$$

3 Results and discussion

The validity of a high-pressure EOS should be test on its shock compression behavior [1–4,8,9]. It is worthwhile to use the improved Tsien's EOS to examine the behavior of C_v along the Hugoniot, the temperature–pressure Hugoniot, the pressure–volume Hugoniot and the U_s–U_P plane, where U_s is the shock wave velocity, and U_P is the particle velocity behind the shock front. These quantities, plotted in Figs. 2, 3, 4 and 5, exhibit physically reasonable behavior. The assumptions of Cowperthwaite and Shaw's, though thermodynamically consistent, were not consistent with the experimental observations taken by Pangilinan [21]. Thus, the results of Cowperthwaite and Shaw's EOS were not included in Figs. 2, 3, 4 and 5.

Figure 2 shows the pressure along the Hugoniot curve, including our theoretical calculations, Lysne and Hardesty's experimental results [4], and Hablot and Soulard's MD simulations [22]. It can be seen clearly that our pressure prediction using the improved Tsien's EOS is consistent with other theoretical and experimental results.

Figure 3 illustrates the variation of particle velocity behind the shock wave front with shock wave velocity along Hugoniot curve. The shock wave velocity range of the Lysne and Hardesty experiment is from 1.5 to 4.0 km/s [4], and the

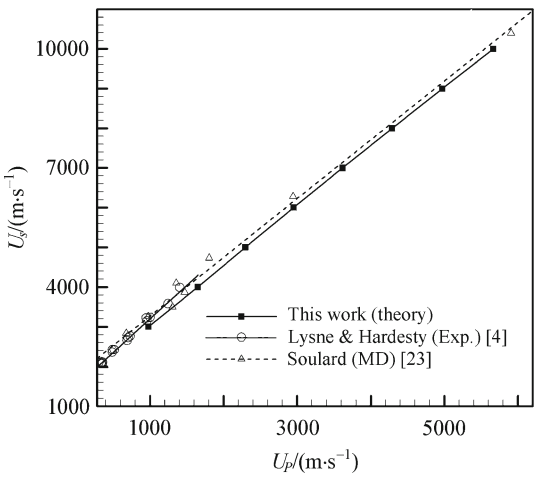

Fig. 3 Shock velocity as a function of particle velocity behind the shock front

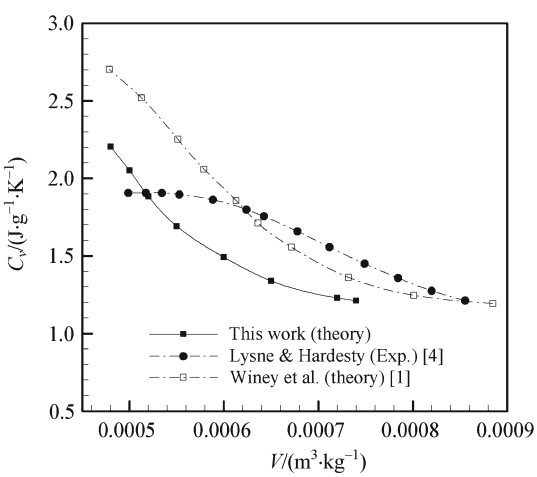

Fig. 4 Specific heat C_v along the Hugoniot curve

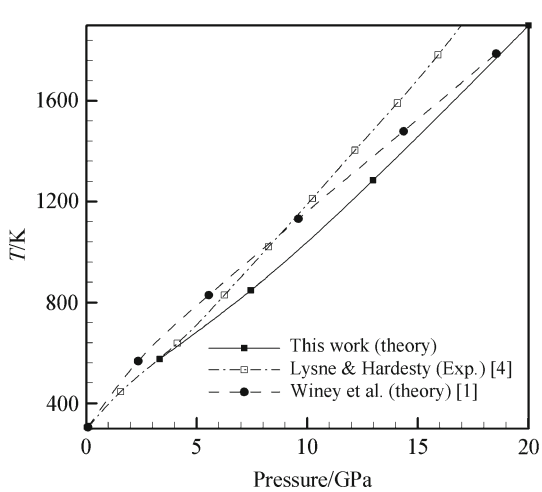

Fig. 5 Temperature along the Hugoniot curve

U_s–U_P relationship of the experiment is (the dimensions of the following U_s and U_P are km/s)

$$U_s = 1.50 + 1.54U_P, \tag{17}$$

Sourlard [23] gave the data of U_s and U_P for shocked nitromethane using direct MD simulation. In the low shock wave velocity regime ($U_s < 4.0$ km/s), the relationship is

$$U_s = 1.20 + 1.95U_P. \tag{18}$$

In the shock wave velocity range of 4.0–10 km/s, that is

$$U_s = 1.95 + 1.39U_P. \tag{19}$$

Taking into account all the data given by Sourlard, the U_s–U_P Hugoniot is

$$U_s = 1.66 + 1.46U_P. \tag{20}$$

Using the improved Tsien's EOS, we got the U_s–U_P Hugoniot

$$U_s = 1.50 + 1.52U_P\,(U_s < 6.0), \tag{21}$$

$$U_s = 1.66 + 1.47U_P\,(6.0 \le U_s < 10.0). \tag{22}$$

Unified these two sets of data, the result is

$$U_s = 1.55 + 1.50U_P. \tag{23}$$

By comparing the U_s–U_P Hugoniots, we can see that our results agree with the experimental data for $U_s < 6.0$ km/s. The intercepts of Eqs. (17) and (21) are the same, and the discrepancy of the slopes of these two equations is 1.3%. In the shock wave velocity range of 6.0–10.0 km/s, our calculation has the same intercept with Sourlard's simulation, and the discrepancy is only 1% (see Eqs. 20, 22).

The specific heat, with its relationship to the thermal accessibility of vibrational modes in the molecule, increases with a decrease of specific volume as expected along the Hugoniot curve (in Fig. 4). The assumptions of specific heat are the same for Winey EOS [1], Lysne and Hardesty EOS [4] and the improved Tsien's EOS, where the specific heat is a function of temperature and volume. The specific heat of Lysne and Hardesty EOS is extrapolated numerically from the experimental data. The improved Tsien's EOS considers that the vibrational modes in the molecule are independent of the system pressure. Therefore, the specific heat is composed of the perfect part and the imperfect one (see Eq. 16). The specific heat of Winey EOS is also composed of two parts similar to the improved Tsien's EOS.

The specific heat of Winey EOS is higher than the data of Lysne and Hardesty EOS and the improved Tsien's EOS. This is due to that Winey et al., although, considered the temperature dependent contributions from the vibrational modes, they used a single Einstein temperature to substitute all the vibrational modes and took inadequate data to fit the perfect

part of the specific heat function. The contributions for nitromethane from the vibrational modes have been calculated by Burcat [20]. The perfect part of specific heat obtained by Winey et al. is larger about 20% than that calculated by Burcat in the range of 350–6,000 K. In the high density regime ($V \leq 0.006\,\mathrm{m}^3/\mathrm{kg}$), the specific heat of Lysne and Hardesty EOS has an incorrect trend, and it should increase with the specific volume decreasing along the Hugoniot curve such as the other two curves in Fig. 4. The contribution for specific heat from the specific volume is very important in high density range. In the ambient conditions regime, they are all consistent.

Figure 5 shows the temperature predictions along the Hugoniot curve using the improved Tsien's EOS. Additionally, we show the data from the Winey EOS [1] and the Lysne and Hardesty EOS [4]. In this figure, the Hugoniot temperatures calculated by the three EOS are remarkably different. This is likely due to the differences in the behavior of C_v for the three EOS developments (see Fig. 4), since the temperature rise due to shock compression depends strongly on the specific heat [2,8]. Temperature predictions from these three EOS developments coincide over the range of lower Hugoniot pressures. However, at higher Hugoniot pressures, the Lysne and Hardesty EOS specific heat predictions are less than the other two EOS, thus the temperatures calculated by this EOS is higher than the two EOS results. The Winey EOS predictions are larger than the results of this work over the pressure range because Winey et al. took the wrong specific heat.

4 Conclusions

The improved Tsien's EOS is an analytical EOS for high pressures and high temperatures, which is developed from kinetic theory and the "exact" numerical solutions of equation of state. This EOS is also a complete equation of state, and can deduce all consistent thermodynamic variables and coefficients. Furthermore, it is a universal EOS with a single parameter (ς), and has nothing to do with specific material. The significant advantage of this EOS is that it does not need fitting parameters by shocked experimental data, but required the L–J potential parameters of molecular, such as compiled in Refs. [14,24]. However, the parameters of Cowperthwaite EOS, Lysne and Hardesty EOS and Winey EOS must fit the experimental data.

To test the improved Tsien's EOS predictions, the Hugoniots of shocked nitromethane calculated by this EOS are compared with earlier EOS works, experiments, and direct MD simulations. In the thermodynamic property calculations, the contributions from vibrational modes have been taken into account. The comparison shows that this EOS can accurately predict the material temperature, pressure, density, and particle velocity behind the shock wave front.

The improved Tsien's EOS has an explicit expression of temperature, and a simple calculation for the state of shocked material. This EOS is used not only for detonation of energetic material, but also for complex computation such as coupling with chemical reaction.

References

1. Winey, J.M., Duvall, G.E., Knudson, M.D., Gupta, Y.M.: Equation of state and temperature measurements for shocked nitromethane. J. Chem. Phys. **113**, 7492–7501 (2000)
2. Cowperthwaite, M., Shaw, R.: $C_V(T)$ equation of state for liquids. Calculation of the shock temperature of carbon tetrachloride, nitromethane, and water in the 100-kbar region. J. Chem. Phys. **53**, 555–560 (1970)
3. Shaw, R.: Calculated shock temperatures of liquid TNT, nitromethane, and four liquid bis(Difluoramino) alkanes. J. Chem. Phys. **54**, 3657–3658 (1971)
4. Lysne, P.C., Hardesty, D.R.: Fundamental equation of state of liquid nitromethane to 100 kbar. J. Chem. Phys. **59**, 6512–6523 (1973)
5. Tsien, H.S.: Thermodynamic properties of gas at high temperatures and pressures. Jet Propulsion **25**, 471–473 (1955)
6. Wentorf, J.R.H., Buehler, R.J., Hirschfelder, J.O., Curtiss, C.F.: Lennard–Jones and devonshire equation of state of compressed gases and liquids. J. Chem. Phys. **18**, 1484–1500 (1950)
7. Zhao, B., Cui, J.P., Fan, J.: Equation of state in high-temperature and high-pressure gases and an improvement of Tsien's EOS. Chin. J. Theor. Appl. Mech. **42**(2), 151–158 (2010)
8. Sheffield, S.A., Duvall, G.E.: Response of liquid carbon disulfide to shock compression: equation of state at normal and high densities. J. Chem. Phys. **79**, 1981–1990 (1983)
9. Sutherland, G.T., Gupta, Y.M., Bellamy, P.M.: Pressure-time profile of multiply shocked carbon-disulfide. J. Appl. Phys **59**, 1141–1146 (1986)
10. Campbell, A.W., Davis, W.C., Travis, J.R.: Shock initiation of detonation in liquid explosives. Phys. Fluids **4**, 498–510 (1961)
11. Walker, F.E., Wasley, R.J.: Initiation of nitromethane with relatively long-duration, low-amplitude shock waves. Combust. Flame **15**, 233–246 (1970)
12. Hardesty, D.R.: An investigation of the shock initiation of liquid nitromethane. Combust. Flame **27**, 229–251 (1976)
13. Winey, J.M., Gupta, Y.M.: Visible absorption spectroscopy to examine shock-induced decomposition in neat nitromethane. J. Phys. Chem. A **101**, 9333–9340 (1997)
14. Hirschfelder, J.O., Curtiss, C.F., Bird, R.B.: Molecular Theory of Gases and Liquids. Wiley, New York (1954)
15. Tsai, D.H.: The virial theorem and stress calculation in molecular dynamics. J. Chem. Phys. **70**, 1375–1382 (1979)
16. Jones, H.D.: Equation of State for Liquid Nitromethane at High Pressures. Shock Compression of Condensed Matter 2003, Portland, Oregon, pp. 149–152 (2004)
17. Sorescu, D.C., Rice, B.M., Thompson, D.L.: Molecular dynamics simulations of liquid nitromethane. J. Phys. Chem. A **105**, 9336–9346 (2001)
18. Liu, H., Zhao, J.J., Ji, G.F., Gong, Z.Z., Wei, D.Q.: Compressibility of liquid nitromethane in the high-pressure regime. Phys. B Condens. Matter **382**, 334–339 (2006)
19. Alper, H.E., Abu-Awwad, F., Politzer, P.: Molecular dynamics simulations of liquid nitromethane. J. Phys. Chem. B **103**, 9738–9742 (1999)

20. Burcat, A.: Thermodynamic properties of ideal gas nitro and nitrate compounds. J. Phys. Chem. Reference Data **28**, 63–130 (1999)
21. Pangilinan, G.I., Gupta, Y.M.: Time-resolved raman measurements in nitromethane shocked to 140 kbar. J. Phys. Chem. **98**, 4522–4529 (1994)
22. Hablot, O., Soulard, L.: Shock decomposition of nitromethane. pp. 857–860. Shock Compression of Condensed Matter-1999. Snowbird, Utah (2000)
23. Soulard, L.: Molecular dynamics and experimental study of shock polarization of nitromethane. In: 12th APS Topical Conference, Shock Compression of Condensed Matter-2001, Atlanta, Georgia, pp. 347–350 (2002)
24. Tee, L.S., Gotoh, S., Stewart, W.E.: Molecular parameters for normal fluids. I&EC Fundam **5**, 12 (1966)